ADVANCED FUNCTIONAL MATERIALS
www.afm-journal.de

Photoresponsive Soft-Robotic Platform: Biomimetic Fabrication and Remote Actuation

Weitao Jiang, Dong Niu, Hongzhong Liu,* Chaohui Wang, Tingting Zhao, Lei Yin, Yongsheng Shi, Bangdao Chen, Yucheng Ding, and Bingheng Lu*

Biomimetic microsystems, which can be driven by various stimuli, are an emerging field in micro/nano-technology and nano-medicine. In this study, a soft and fast-response robotic platform, constituted by PDMS/graphene-nanoplatelets composited layer (PDMS/GNPs) and pristine PDMS layer, is presented. Due to the differences in coefficient of thermal expansion and Young's modulus of the two layers, the bilayer platform can be driven to bend to the PDMS/GNPs side by light irradiation. The robotic platform (1 mm in width and 7 mm in length) can be deflected about 1500 μm by near infrared irradiation (nIR)(808 nm in wavelength) within 3.4 s, and excellent reversibility and repeatability in actuation are also revealed by sweeping and multi-cycle light irradiation. The experiments also show that, the presented bilayer platform in various shapes, that is, fish-like shapes, can float and swim to perspective location in fluid (i.e., water), whose moving directions and velocities can be remotely adjusted by light, indicating an excellent light-actuation ability and well controllability. The results may be not only hopeful in developing light-driven drug-delivery platform, but also the bio-robotic microgrippers applying in vivo and in vitro.

1. Introduction

There is a growing interest in the design of microrobots or biomimetic micro-motors in micro/nano-medicine and nano-technology, especially the realization of functionalities mimicking biological systems with lifelike or biomimetic motions in response to applied external controllable stimuli. As the key part in microrobots, stimuli-responsive materials have drawn enormous attention due to their brilliant intriguing shape or volume recovery properties under different external stimuli, which are helpful for creating mechanical motion rapidly and precisely. Many stimuli-responsive polymers, including hydrogel,[1,2] electro-active polymers (EAPs),[3,4] shape memory polymers,[5] and polymeric nanocomposites (composited with gold nanorods,[6,7] carbon nanotubes (CNTs),[8,9] graphene,[10,11] etc.), have been investigated and developed. Accompany with the development of stimulus-responsive materials, various types of external stimulus, including electric,[12,13] heat,[14–16] light,[17,18] magnetic,[19–21] chemical stimulus,[22] pneumatic stimulus,[23] and so forth, have been successfully employed to develop biomimetic or bio-inspired micro-robotic systems applying in microjets,[16] microgrippers,[24,25] drilling of tissues,[26] drug and cell delivery,[27,28] fixing cancer cells,[29] artificial muscles,[30] and some other smart microstructures.

Because of their ability in wireless/remote control, low noise, localized driven ability rather than whole-field driven,[31] light-driven microrobots have attracted more and more attention in novel micro-bio-robots or micro-motors for biological use. For example, for the minimally invasive medicine applications, the microrobots must exhibit locomotion and controlled interaction with their environment, which should be able to reach a targeted area under the direct supervision and control of an external user. Due to its excellent penetration ability in biological tissues (can be over several centimeters[32]), near infrared (nIR) light provides a promising approach to remotely actuate the microrobots in bodies, which may find applications in the development of novel micro-bio-robots or biomimetic micro-motors in vivo and in vitro.

Graphene, due to its excellent electrical and thermal conductivity, high surface area, and high flexibility, has been employed to perform various actuation based on graphene polymeric nanocomposites, that is, stimulated by electrical,[33,34] electrochemical,[11,35] and optical energy.[10] Because of its photothermal effect and high thermal conductivity, graphene and its composites show promising photoresponsive properties. Panchapakesan[31] reported a large light-induced reversible and elastic response of graphene nanoplatelets (GNPs) polymer composites which is composited with GNPs and polydimethylsiloxane (PDMS), and developed a two-axis submicrometer resolution positioning stage. Wu[36] developed a bimorph configuration which was constituted with chemically modified polyethylene (PE) films and a mixture of large-area graphene-chitosan, behaving as a transparent soft actuator that expanded under nIR irradiation. Wang[37] developed light-driven hand-shape

Dr. W. Jiang, D. Niu, Prof. H. Liu, Prof. C. Wang, T. Zhao, Dr. L. Yin, Dr. Y. Shi, Dr. B. Chen, Prof. Y. Ding, Prof. B. Lu
State Key Laboratory for Manufacturing Systems Engineering
Xi'an Jiaotong University
Xi'an 710049, China
E-mail: wtjiang@mail.xjtu.edu.cn; hzliu@mail.xjtu.edu.cn

DOI: 10.1002/adfm.201402070

matrix by combining reduced graphene oxide (rGO) nanosheets and elastomeric proteins such as elastin-like polypeptides (ELPs) and achieved joint-like flexing motions and crawlers. For the graphene-based soft platform which can be remotely driven by light, however, the study is far more from mature. Researchers are seeking for new fabrication methods to pave the way to applications, e.g., the responsive platforms should be broadened to adapt to more universal working environments, rather than liquid solution that most studied in previous work, the response time should be further shortened to a few seconds, and etc.

Herein, we present an effective method for the fabrication of a polymeric bilayer biomimetic platform, which can be light-actuated both in air and water. The bilayer platform is constituted by a pure PDMS layer and a PDMS/GNPs composited layer, in which each layer has a different coefficients of thermal expansion (CTE) and Young's modulus due to the existence of the GNPs. The polymeric bilayer can be reversibly deflected at millimeter scale in response to near infrared (nIR) irradiation, which can be attributed to the photothermal effect of graphene. The deflection performances, i.e., deflection magnitude and response time, are determined by the light intensity and GNPs concentration.

Furthermore, a biomimetic microfish, based on the bilayer platform, is designed and prepared, which can move forward, backward, and turn around in water under nIR irradiation, to mimic fish swimming in nature. It is well known that, fish swimming can be attributed to the exerting force against surrounding water. Most fishes generate thrust using lateral movements of their body and caudal fin. The force exerted on the water by such motion cancels out laterally, but generate a net force backwards which in turn pushes the fish forward through the water, as **Figure 1**a shows. Inspired by fish swimming, we construct a fish-like platform based on soft materials (e.g., PDMS and its composites), which can deform in local expected places, similar to the locomotion of fish "caudal fin", to beat water and push itself to the opposite direction, as shown in Figure 1b. The desired local deformation of the proposed biomimetic platform is induced by nIR light irradiation, which is promising for remote control. The artificial microfish may be not only hopeful in developing light-driven drug-delivery platform, but also the bio-robotic microgrippers applying in vivo and in vitro.

2. Results and Discussion

2.1. Design and Fabrication of Polymeric Bilayer

Figure 2a schematically illustrates the fabrication process of polymeric bilayer microstructure. The process is facile and scalable, which only involves scraping coating and spin coating processing for bottom and upper layer respectively. The details of the fabrication process are described in the Experimental Section.

Because of the existence of GNPs, the composited PDMS/GNPs layer takes different CTE and Young's modulus in contrast to pristine PDMS layer. The differences in CTEs and Young's modulus determine the actuation properties of the PDMS-PDMS/GNPs bilayer platform. In Figure 2b, nIR light (808 nm in wavelength) irradiates from the side of pristine PDMS layer. While graphene shows decreasing absorption from visible to nIR,[38] there is a brilliant photothermal conversion efficiency in the band of nIR, which has arose tremendous interest in biomedical applications, such as drug delivery[39] and photothermal and photo-dynamic therapies.[40,41] When the nIR irradiation is absorbed by the GNPs, the polymeric bilayer experiences a temperature elevation and will deflect to the PDMS/GNPs side due to the different thermal expansions of each layer.

2.2. Characterization of Polymeric Bilayer Microstructures

Figure 2c shows the Raman spectroscopy of the adopted GNPs at 633 nm excitation. The GNPs displayed well-known D-band peaks near 1350 cm^{-1}, G-band peaks near 1580 cm^{-1} and 2D-band peaks near 2700 cm^{-1}. The observed frequency shifts in all peaks are in line with the configuration of multilayer graphene,[42,43] which can also be verified by the height ratio (0.33)

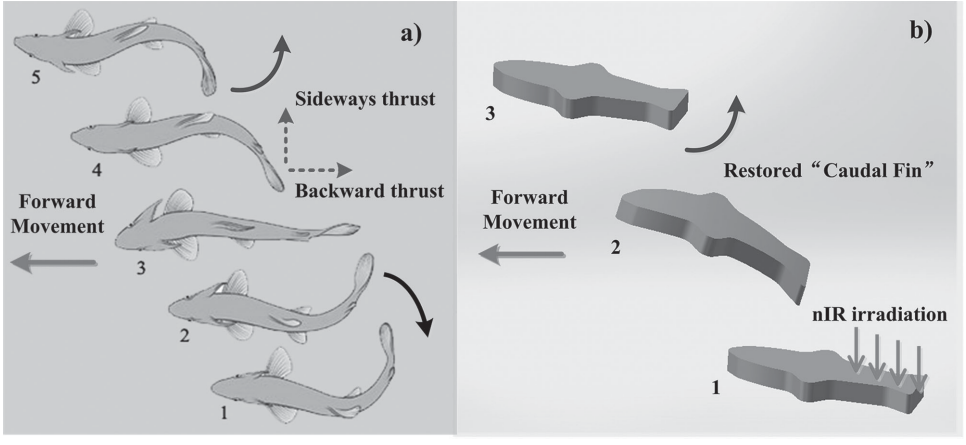

Figure 1. a) Fish swims in water through the movement of its caudal fin. b) A designed microfish which can swim to any directions when locally stimulated by nIR irradiation, with a similar mechanism to fish swimming.

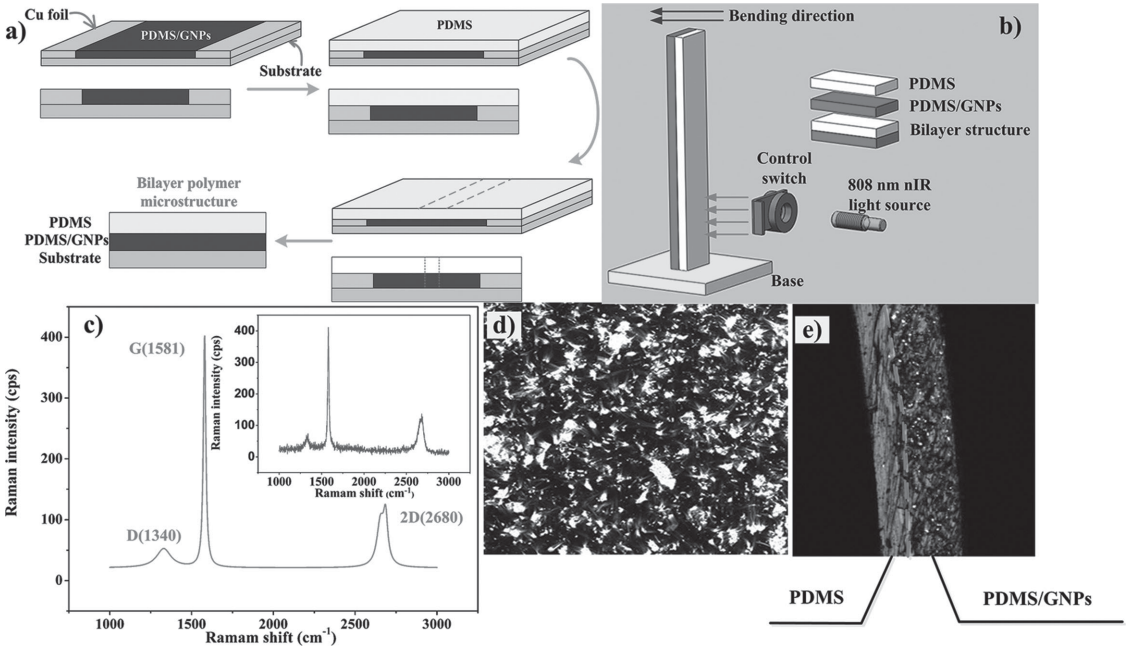

Figure 2. a) Fabrication scheme of polymeric bilayer microstructure. b) Diagram of bilayer platform actuation. The bilayer structure was vertically anchored on a base and would bend to the PDMS/GNPs side under nIR irradiation. c) Raman microscopy of GNPs, indicating the adopted GNPs is multi-layered. d,e) Confocal microscopy of samples with 2 wt% GNPs concentration, revealing the uniform and densely distribution in PDMS film.

of the 2D peak to G peak Raman spectroscopy data at 633 nm excitation. Figure 2d,e illustrates the optical image of the fabricated PDMS-PDMS/GNPs microstructure. It is observed that, the thickness of the bilayer is 130 μm in total, in which the PDMS/GNPs composited layer is 80 μm, and the pristine PDMS is 50 μm.

2.3. Photothermal Actuation of the Polymeric Bilayer

In order to investigate the photoresponsive properties of our polymeric bilayer platform, pieces of polymeric bilayer with different GNPs concentration were prepared, with 7 mm in length and 1mm in width. All the samples were actuated by nIR irradiation in air, as shown in **Figure 3**a. In order to reveal the light absorption and light-thermal conversion, an infrared camera was employed to record the real-time temperature of the samples during the actuation cycle, as Figure 3b shows. Taking the sample containing 5 wt% GNPs in PDMS/GNPs layer for example, it is evident that the temperature increases rapidly and finally gets to steady value (by 60 °C increment) within 5 s. Figure 3c shows the temperature profile as a function of irradiation time. Rapid temperature increase and decay are clearly observed for each polymeric bilayer. The maximum temperature and corresponding temperature response time (that is, the time needed to get to the maximum temperature when irradiation) shows incremental as the increase of GNPs concentration.

The mechanical deflection of each sample was also measured to reveal the relationship between deflection and light-thermal conversion. As illustrated in Figure 3d, apart from the single layer pristine PDMS, all the polymeric bilayers exhibited photomechanical response to the nIR irradiation owing to the brilliant photothermal effect of graphene. The deflection is enhanced with the augment of GNPs concentration and reaches the maximum (about 1500 μm) at 5 wt% concentration, which approaches the result obtained by Wu group.[36] To further reveal the response to light stimulus, temperature range and deflection were normalized. The deflection response time (that is, the time needed to get to 90% of maximum deflection when irradiation) of each polymeric bilayer is extracted, as shown in Figure 3e,f. It is noticed that the deflection response time is highly dependent on the the GNPs concentration, which is relevant to the enhancement of light-temperature conversion for higher GNPs concentration, and faster response occurs for the sample with higher GNPs concentration. The sample with 2 wt% GNPs concentration shows a faster deflection than that with 5 wt%, which can be explained by the small difference in temperature change (about 5 °C) but a large difference in deflection between 2 wt% and 5 wt% concentration sample. As the case for CNT microactuators with nearly 20 s in response time,[8] our polymeric bilayer microactuator displays a much faster response (3.4 s), which approaches the results of the graphene electrochemical actuator proposed by Qu.[35] For the microactuator made by PDMS/GNPs single layer, the deflection experienced with the same tendency, while with a much smaller deflection, which may because only thermal expansion effect contributes to the deflection for single layer. As contrast, due to its poor nIR absorption, there is no obvious deflection can be observed for pristine PDMS when irradiation.

To elucidate the deflection enhancement as nIR intensity and GNPs concentration increasing, a series of light intensity, ranging from 2.1 mW mm^{-2} to 29.5 mW mm^{-2} was employed to actuate each polymeric bilayer microactuator. **Figure 4**a

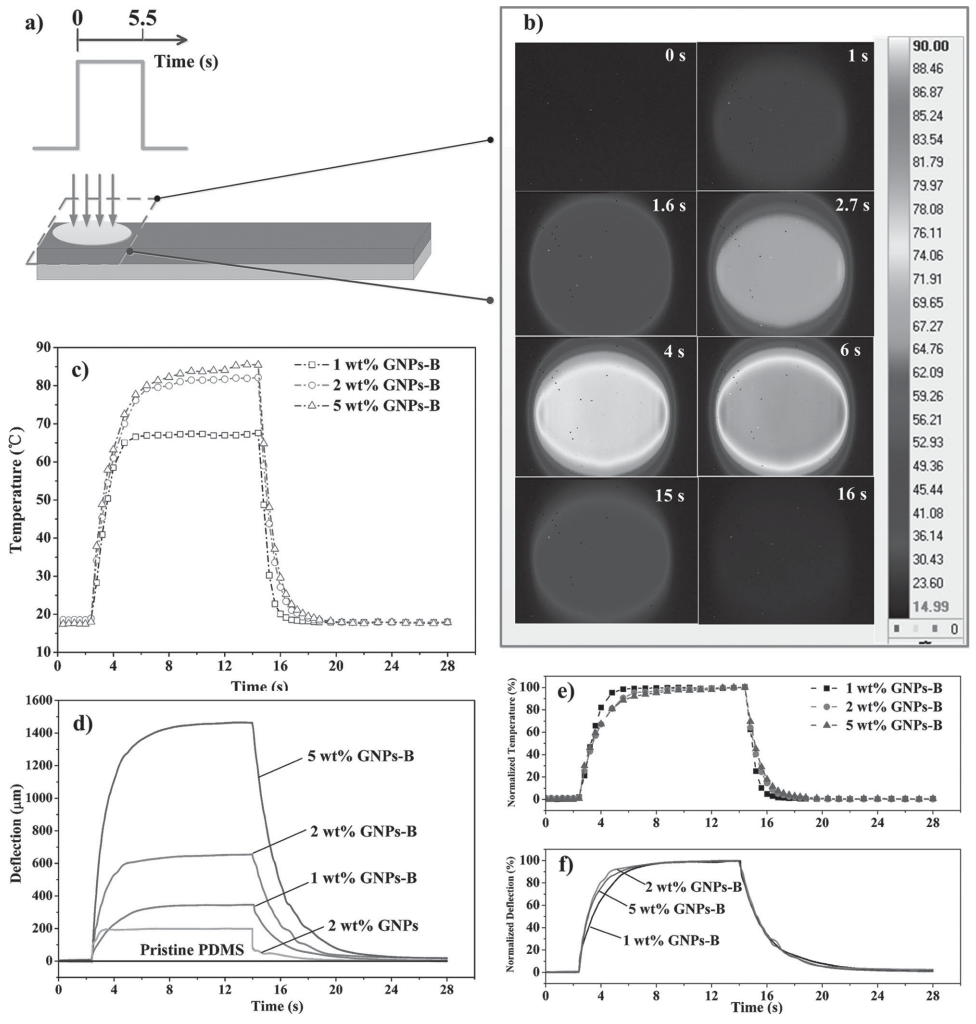

Figure 3. a) Scheme of polymeric bilayer microactuator in air. By nIR irradiation on local area, the temperature on the irradiated area was elevated, and deflection is induced by the differences in coefficients of thermal expansion and Young's modulus. b) Temperature fluctuation during the irradiation for the polymeric bilayer microactuator with 5 wt% GNPs concentration. c) Temperature profile at the irradiation area of polymeric bilayer microstructures as light is turned on (at 2.4 s) and off (at 14.4 s) for different GNPs concentrations. d) Deflection induced by nIR irradiation. e,f) Normalized temperature and deflection at different GNPs concentration.

exhibits the deflection as a function of light intensity for samples with different GNPs concentration. For each polymeric bilayer microactuator, the deflection was gradually enhanced as the increase of the applied light intensity, and deflection can be up to 1500 μm at the light intensity of 29.5 mW mm^{-2} for the sample with 5 wt% GNPs. According to the measured temperature maps when irradiation, the final temperature was gradually elevated as light intensity rising, as shown in Figure 4c and dependent on the GNPs concentration as well. Meanwhile, the deflection of each polymeric bilayer sample is closely related to the temperature elevation during light intensity rising, as shown in Figure 4b, which further confirm the temperature change, induced by photothermal effect of graphene, is the motivation to the deflection. From Figure 4b,c, it can be concluded that, a controllable deflection can be realized by regulating light absorption through light intensity and GNPs concentration, which may find applications in microactuators fabrication and their remote control.

It is well known that, hysteresis and repeatability are the key indicators to evaluate the actuators performance. To evaluate the hysteresis of our PDMS/GNPs-PDMS bilayer microactuators, the deflections were measured by light-intensity sweeping. As shown in Figure 4d, bilayer microactuator with 1 wt% GNPs concentration was selected to record static deflection under different level of nIR illumination between 0 mW mm^{-2} and 29.5 mW mm^{-2}. Figure 4e shows the static deflection as a function of nIR light intensity extracted from Figure 4d. In the sweep-up process, the microactuator experienced an ascending deflection, while in the sweep-down process, the deflection gradually decreased. A dimensionless parameter $\delta\% = |(\delta_{as} - \delta_{de})/\delta_{max}|$ is defined to depict hysteresis in the light intensity-deflection curves, where δ_{as}, δ_{de}, and δ_{max} denote the deflection induced by different level of ascending and decreasing light intensity, and maximum deflection respectively. As the schematic illustration in Figure 4e, $\delta\%$ is varied between 1.85% and 3.13%, which confirms that our polymeric bilayer microactuator shows

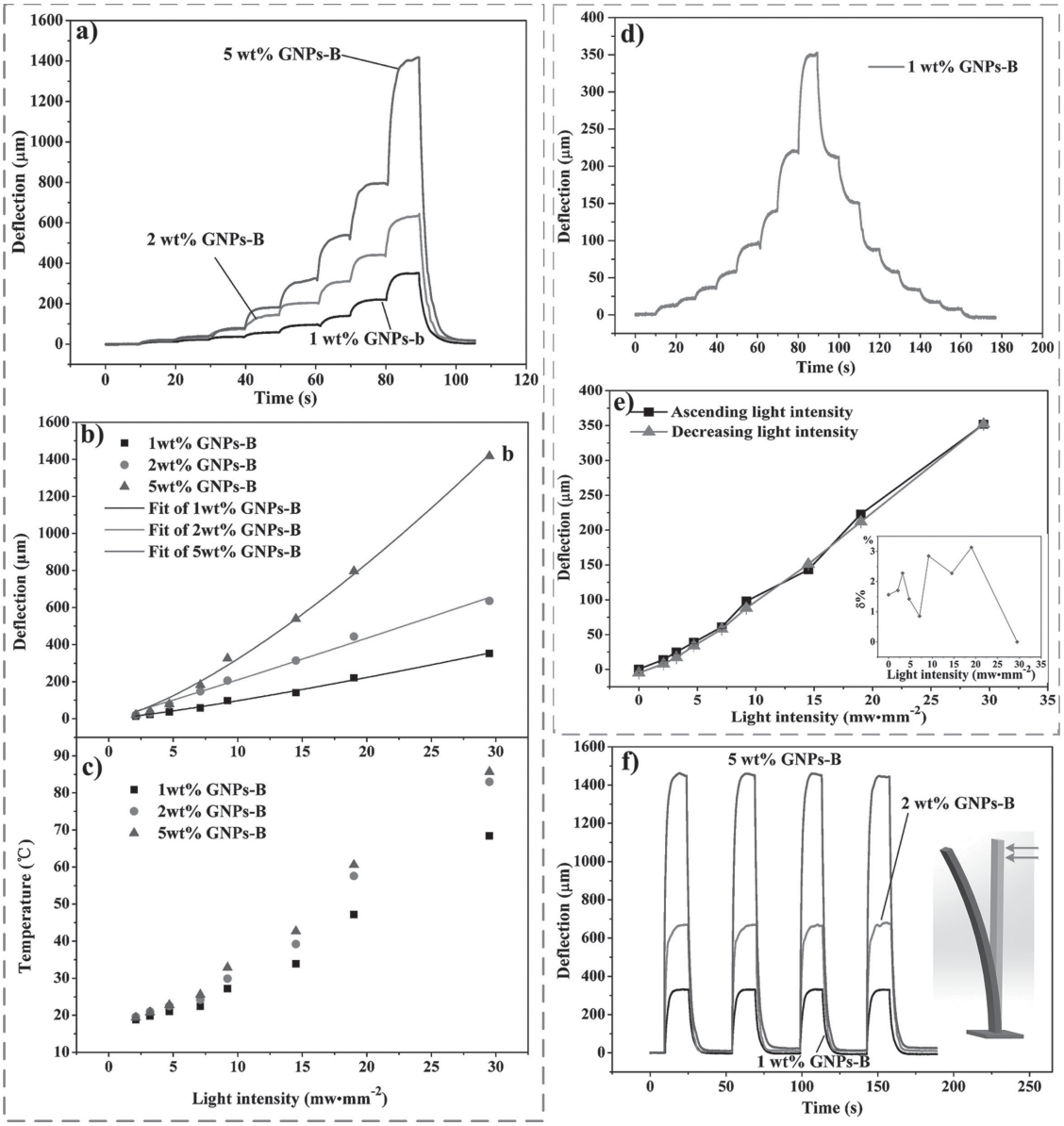

Figure 4. a) Deflection enhancement as a function of nIR intensity and GNPs concentration, which was induced by light intensity ranging from 2.1 mW mm^{-2} to 29.5 mW mm^{-2} in air. b) Maximum deflection as a function of light intensity. c) Temperature profile of bilayer microactuator, which is dependent on light intensities and GNPs concentrations. d) Static deflection of microactuator with 1 wt% GNPs concentration as a function of nIR intensity. In the sweep-up process, the microactuator experienced a ascending deflection, while in the sweep-down process, the deflection gradually decreased, indicating a great reversibility of our bilayer microactuator. e) Hysteresis loop of the deflection shown in (d). δ% is varied between 1.85% and 3.13%. f) Repeatable actuation of the bilayer microactuator induced by multicycle 808 nm nIR irradiation.

a great reversibility under complicating operating conditions. Another parameter to characterize the similarity of sweep-up and sweep-down deflection curves is the coefficient of correlation $r = 0.999$, indicating that these two trends significantly correlate, which show that our polymeric bilayer microactuator experience a good reversibility (no obvious hysteresis) under reciprocating light intensity.

The repeatability of the bilayer microactuators was also investigated by multicycle actuation, as Figure 4f indicates. All the multicycle actuations of these three bilayer polymer microactuators show an excellent repeatability, which indicate that our polymeric bilayer microactuator is qualified with well repeatability.

2.4. Microfish Swimmer: Remotely Driven by nIR Irradiation

For microrobotics, it is more interesting if it can work in various environments. Figure 3, 4 clearly reveal the remote actuation of the polymeric bilayer microactuator in air. In this part, we will show the remote actuation can also perform in a liquid environment, that is, water.

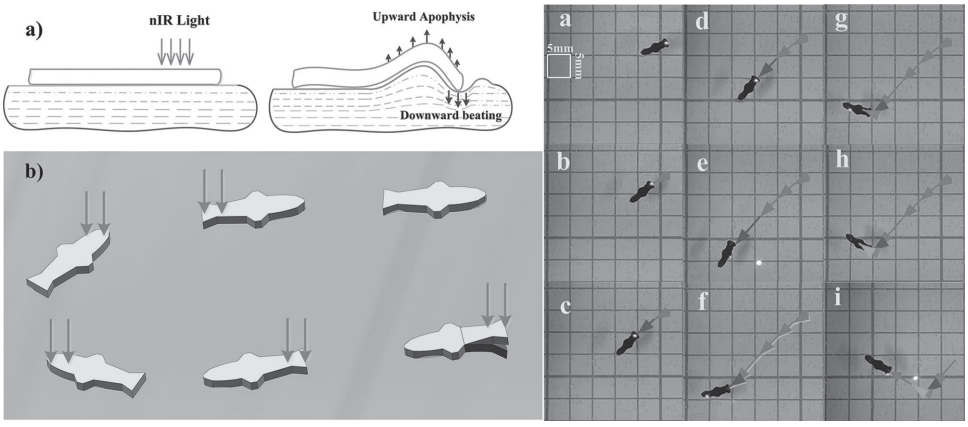

Figure 5. a) Diagram to demonstrate the microfish deflection in a water film. b) An artificial microfish to mimic fish swimming. By adjusting the position of irradiation spot, the artificial microfish can perform various motions, including forward, backward, and turning around, to get to perspective position quickly, which may find applications in drug delivery.

A fish-like bilayer actuator (named microfish), was designed to imitate fish swimming in water. In order to easily observe the microfish deflection in water, a water film was employed to restrict the microfish in the film region. As shown in **Figure 5**a, when nIR light illuminates on the tail of the microfish, the tail experiences downwards movement, as shown in Supporting Information 1. In addition, the same condition could occur when nIR illuminates on the edge of the microfish. It should be noted that, when the microactuator is actuated by nIR in water, there is an obvious heat transfer from the sample to water (as Figure 1 in Supporting Information shows), and the heat dissipates much more rapidly in water than that in air. Due to the smaller temperature increase under nIR illumination and larger resistance to deflection in water, the deflection in water is less than that in air.

In a water pool, the local deflection of the microfish induces a force disequilibrium, which results in the microfish swimming. For example, the tail downwards movement could push the microfish swimming forward, which is similar to the tail swinging of a real fish; the edge deflection of the microfish could induce the turning around of the microfish. The sequence aquatic movement of the microfish is shown in Supporting Information 2. When nIR light was turned on and illuminating on the microfish, the microfish immediately moved towards the direction opposite to the shinning spot. The movement can be mainly attributed to the local deflection of the shinning area, which induces immidiatly water beating and push the artificial fish to the opposite direction, similar to fish swimming. By the same way, the microfish can also turn around under light irradiation. So, the microfish made by polymeric bilayer can swim to anywhere we prospect, which can be used for drug delivery. We believe that the polymeric bilayer actuator can enjoy various deflecting tendencies by control the light source which not only helps for expansion of biometric mechanism but also contributes to a new method for medicine transportation in medical application.

In addition, it is no doubt that heat transfer from the micro fish to water occurs (as Figure 1 in Supporting Information shows), and the induced thermal convection may also contribute to the microfish swimming.

3. Conclusion

In this paper, we present the design and fabrication of a bilayer robotic platform which can be driven by nIR light irradiation. Due to the differences in CTE and Young's modulus of the two layers, the bilayer robotic platform can deflect under nIR light irradiation. The platform can be bent with a deflection about 1500μm within 3.4 s by nIR light irradiation in air, which exhibits a much faster response than previous studies. To evaluate the deflection hysteresis, light intensity sweeping, 2.1 to 29.5 mW mm^{-2}, was employed. The deflection hysteresis loop, with δ% less than 3.13% and $r = 0.999$ (the coefficient of correlation in sweep-up and sweep-down), indicates that the robotic platform experiences a good reversibility. Multi-cycle actuation shows an excellent driving repeatability, which may find applications in developing novel remote-driven actuators. To further test the actuation ability of the platform, microfish, which can swim in water to any directions, that is, forward, backward, and turning around, was fabricated, indicating great potential applications in controllable delivery ability by remote control. We believe that the robotic platform can further be explored for many applications, such as biomimetic research, microcantilevers, micro/nanorobotics, drug delivery, implanting medical robots, and so on.

4. Experimental Details

Materials: GNPs were purchased from JiangNan Graphene Research Institute and were directly used in their original form. PDMS obtained from Dow Corning (Sylgard 184) was used as the host matrix. PDMS is a two-part solvent free flexible silicone organic polymer in the form of a base compound with a separate hydrosilane curing agent that acts as a crosslinker. And a Raman spectroscopy data at 633 nm excitation was used to characterize the GNPs.

Microfabrication of Polymeric Bilayer Microactuator: PDMS/GNPs composite was prepared by weighing desired amount of GNPs and adding to the PDMS crosslinker. The GNPs/crosslinker compound were mixed for 10 min and degassed for 30min. Then the PDMS base compound was added at a ratio of 10:1 to the PDMS crosslinker and mixed for 10 min. To remove the trapped air pockets, prepared polymer was degassed for 30 min to achieve GNPs/PDMS nanocomposites.

Pure PDMS solution was configured by the PDMS base compound and crosslinker at a ratio of 10:1. After fully stirred for 10 min, the polymer was degassed for 30 min. Appropriate amount of GNPs/PDMS liquid polymer was poured on 2 cm × 2 cm substrate with scratching process by doctor blade and cured at 65 °C for 4 h to fabricate the bottom GNPs/PDMS layer. Its thickness is 80 μm.With a standard spin coating process (820 rpm, 60 s), 50μm-thick PDMS layer was deposited on the GNPs/PDMS layer to fabricate the bilayer structure. Polymeric bilayer microactuator (1 mm × 7 mm) was cut to make further measurement.

nIR Actuation of the Polymeric Bilayer: To observe the deflection of polymeric bilayer actuator, we chose a nIR light source with the wavelength of 808 nm.The light density was recorded with THORLAB PM200D intensity meter. The PDMS layer was shined by nIR light spot (2 mm × 4.5 mm). A KEYENCE displacement sensor was used to record the tip deflection of this polymeric bilayer microactuator. We also measured the tip deflection of this configuration under different light density. FLIR SC7300M infrared camera was employed to measure the real-time temperature change of each polymeric bilayer microactuator upon nIR light irradiation.

Supporting Information

Supporting Information is available from the Wiley Online Library or from the author.

Acknowledgements

This work is supported by National Natural Science Foundation of China (No. 91323303, 51305337, 51275400), National Science and Technology Project (No. 2011ZX04014071, SK201401A53–01, and CERS-1-X1), the Fundamental Research Funds for the Central Universities and China Postdoctoral Science Foundation (No. 2012M520081, 2013M530419, 2013M530424 and 2013M532035). This work is partially sponsored by the Natural Science Foundation of Shaanxi Province (2013JQ7021) and the Specialized Research Fund for the Doctoral Program of Higher Education (20130201120036).

Received: June 23, 2014
Revised: August 25, 2014
Published online: September 29, 2014

[1] P. J. Glazer, J. Leuven, H. An, S. G. Lemay, E. Mendes, *Adv. Funct. Mater.* **2013**, *23*, 2964.
[2] L. Qiu, D. Liu, Y. Wang, C. Cheng, K. Zhou, J. Ding, V. T. Truong, D. Li, *Adv. Mater.* **2014**, *26*, 3333.
[3] F. Carpi, R. Kornbluh, P. Sommer-Larsen, G. Alici, *Bioinsp. Biomim.* **2011**, *6*, 045006.
[4] B. Bhandari, G. Y. Lee, S. H. Ahn, *Int. J. Precision Eng. Manufact.* **2012**, *13*, 141.
[5] Z. Yu, Q. Zhang, L. Li, Q. Chen, X. Niu, J. Liu, Q. Pei, *Adv. Mater.* **2011**, *23*, 664.
[6] P. Wang, L. Zhang, Y. N. Xia, L. M. Tong, X. Xu, Y. B. Ying, *Nano lett.* **2012**, *12*, 3145.
[7] A. M. Alkilany, L. B. Thompson, S. P. Boulos, P. N. Sisco, C. J. Murphy, *Adv. Drug. Delivery Rev.* **2012**, *64*, 190.
[8] S. Lu, Y. Liu, N. Shao, B. Panchapakesan, *Nanotechnology* **2007**, *18*, 065501.
[9] X. B. Zhang, Z. B Yu, C. Wang, D. Zarrouk, J. W. T. Seo, J. C. Cheng, A. D. Buchan, K. Takei, Y. Zhao, J. W. Ager, J. J. Zhang, M. Hettick, M. C. Hersam, A. P. Pisano, R. S. Fearing, A. Javey, *Nat. Commun.* **2014**, *5*, 2983.
[10] J. Loomis, B. King, T. Burkhead, P. Xu, N. Bessler, E. Terentjev, B. Panchapakesan, *Nanotechnology* **2012**, *23*, 045501.
[11] J. J. Liang, L. Huang, N. Li, Y. Huang, Y. P. Wu, S. L. Fang, J. Y. Oh, M. Kozlov, Y. F. Ma, F. F. Li, R. Baughman, Y. S. Chen, *ACS nano.* **2012**, *6*, 4508.
[12] M. Deng, S. G. Kumbar, L. S. Nair, A. L. Weikel, H. R. Allcock, C. T. Laurencin, *Adv. Funct. Mater.* **2011**, *21*, 2641.
[13] L. Z. Chen, C. H. Liu, K. Liu, C. Meng, C. Hu, J. Wang, S. S Fan, *ACS Nano* **2011**, *5*, 1588.
[14] J. S. Kim, D. Y. Lee, J. S. Koh, G. P. Jung, K. J. Cho, *Smart Mater. Struc.* **2014**, *23*, 015011.
[15] E. Y. Erdem, Y. M. Chen, M. Mohebbi, J. W. Suh, G. T. Kovacs, B. B. Darling, K. F. Bohringer, *J. Microelectromech. Syst.* **2010**, *19*, 433.
[16] V. Magdanz, G. Stoychev, L. Ionov, S. Sanchez, O. G. Schmidt, *Angew. Chem. Int. Ed.* **2014**, *53*, 2673.
[17] S. Fusco, M. S. Sakar, S. Kennedy, C. Peters, R. Bottani, F. Starsich, A. Mao, G. A. Sotiriou, S. Pané, S. E. Pratsinis, D. Mooney, B. J. Nelson, *Adv. Mater.* **2014**, *26*, 952.
[18] G. Ugur, J. Chang, S. Xiang, L. Lin, J. Lu, *Adv. Mater.* **2012**, *24*, 2685.
[19] P. J. Vach, N. Brun, M. Bennet, L. Bertinetti, M. Widdrat, J. Baumgartner, S. Klumpp, P. Fratzl, D. Faivre, *Nano Lett.* **2013**, *13*, 5373.
[20] S. Tottori, L. Zhang, F. Qiu, K. K. Krawczyk, O. A. Franco, B. J. Nelson, *Adv. Mater.* **2012**, *24*, 811.
[21] V. Magdanz, S. Sanchez, O. G. Schmidt, *Adv. Mater.* **2013**, *25*, 6581.
[22] J. Liu, Z. Wang, X. J. Xie, H. H. Cheng, Y. Zhao, L. T. Qu, *J. Mater. Chem.* **2012**, *22*, 4015.
[23] R. V. Martinez, J. L. Branch, C. R. Fish, L. Jin, R. F. Shepherd, R. M. D. Nunes, Z. Suo, G. M. Whitesides, *Adv. Mater.* **2013**, *25*, 205.
[24] E. Gultepe, J. S. Randhawa, S. Kadam, S. Yamanaka, F. M. Selaru, E. J. Shin, A. N. Kalloo, D. H. Gracias, *Adv. Mater.* **2013**, *25*, 514.
[25] T. G. Leong, C. L. Randall, B. R. Benson, N. Bassik, G. M. Stern, D. H. Gracias, *Proc. Natl. Acad. Sci. U.S.A.* **2009**, *106*, 703.
[26] A. A. Solovev, W. Xi, D. H. Gracias, S. M. Harazim, C. Deneke, S. Sanchez, O. G. Schmidt, *ACS Nano* **2012**, *6*, 1751.
[27] X. Zhao, J. Kim, C. A. Cezar, N. Huebsch, K. Lee, K. Bouhadir, D. J. Mooney, *Proc. Natl. Acad. Sci. U.S.A.* **2011**, *108*, 67.
[28] T. Garg, S. Singh, A. K. Goyal, *Crit. Rev. Ther. Drug Carrier Syst.* **2013**, *30*, 369.
[29] D. Kagan, M. J. Benchimol, J. C. Claussen, E. Chuluun-Erdene, S. Esener, J. Wang, *Angew. Chem. Int. Ed.* **2012**, *51*, 7519.
[30] J. Foroughi, G. M. Spinks, G. G. Wallace, J. Oh, M. E. Kozlov, S. Fang, T. Mirfakhrai, J. D. W. Madden, M. Shin, S. J. Kim, R. H. Baughman, *Science* **2011**, *334*, 494.
[31] J. Loomis, X. Fan, F. Khosravi, P. Xu, M. Fletcher, R. W. Cohn, B. Panchapakesan, *Sci. Rep.* **2013**, *3*,1900.
[32] Q. Tian, M. Tang, Y. Sun, R. Zou, Z. Chen, M. Zhu, S. Yang, J. Wang, J. Wang, J. Hu, *Adv. Mater.* **2011**, *23*, 3542.
[33] U. Kim, J. Kang, C. Lee, H. Y. Kwon, S. Hwang, H. Moon, J. C. Koo, J. D. Nam, B. H. Hong, J. B. Choi, H. R. Choi, *Nanotechnology* **2013**, *24*, 145501.
[34] S. E. Zhu, R. Shabani, J. Rho, Y. Kim, B. H. Hong, J. H. Ahn, H. J. Cho, *Nano Lett.* **2011**, *11*, 977.
[35] X. Xie, L. Qu, C. Zhou, Y. Li, J. Zhu, H. Bai, G. Shi, L. Dai, *ACS Nano* **2010**, *4*, 6050.
[36] C. Wu, J. Feng, L. Peng, Y. Ni, H. Liang, L. He, Y. Xie, *J. Mater. Chem.* **2011**, *21*, 18584.
[37] E. Wang, M. S. Desai, S. W. Lee, *Nano Lett.* **2013**, *13*, 2826.
[38] G. K. Lim, Z. L. Chen, J. Clark, R. G. S. Goh, W. H. Ng, H. W. Tan, R. H. Friend, P. K. H. Ho, L. L. Chua, *Nat. Photonics* **2011**, *5*, 554.
[39] Y. Pan, H. Bao, N. G. Sahoo, T. Wu, L. Li, *Adv. Funct. Mater.* **2011**, *21*, 2754.
[40] K. Yang, S. Zhang, G. Zhang, X. Sun, S. T. Lee, Z. Liu, *Nano Lett.* **2010**, *10*, 3318.
[41] Y. Zhao, L. Song, Z. P. Zhang, L. T. Qu, *Energy Environ. Sci.* **2013**, *6*, 3520.
[42] A. C. Ferrari, *Solid. State. Commun.* **2007**, *143*, 47.
[43] J. Loomis, B. King, B. Panchapakesan, *Appl. Phys. Lett.* **2012**, *100*, 073108.